Effective plasmonic mode-size converter

Hae-Ryeong Park,[1] Jong-Moon Park,[2] Min-su Kim,[3] Jung Jin Ju,[3] Jung-Han Son,[1] and Myung-Hyun Lee[1,*]

[1]*School of Information and Communication Engineering, Sungkyunkwan University, Suwon, Gyeonggi-do 440-746, Korea*
[2]*CAE Group, LCD R&D Center, LCD Business, Samsung Electronics Co. Ltd., San 24 Nongseo-Dong, Giheung-Gu, Yongin-City, Gyeonggi-Do, 446-711 Korea*
[3]*Electronics & Telecommunications Research Institute, 161 Gajong-dong, Yusong-gu, Daejeon 305-701, Korea*
[*]*mhlee@skku.edu*

Abstract: Plasmonic mode-size converters (PMSCs) for long-range surface plasmon polaritons (LR-SPPs) at the wavelength of 1.55 μm are presented. The PMSC is composed of an insulator-metal-insulator waveguide (IMI-W), a laterally tapered insulator-metal-insulator-metal-insulator waveguide (LT-IMIMI-W), and an IMIMI-W in series. The mode-intensity sizes of the LR-SPPs for the IMI-W and the IMIMI-W were not only calculated using a finite element method but were also experimentally measured. The propagation losses of the IMI-W and the IMIMI-W as well as the coupling losses between them were analyzed by the cut-back method to investigate the effect of LT-IMIMI-Ws. By using the PMSC with a $\sim$27 $^\circ$ angled LT-IMIMI-W, the coupling loss between a polarization-maintaining fiber and a 3 μm-wide IMIMI-W was reduced by $\sim$3.4 dB. Moreover, the resulting mode-intensity in the output of the PMSC was squeezed to $\sim$35% of the mode-intensity in the input IMI-W. The PMSC may be potentially useful for bridging micro- to nano-plasmonic integrated circuits.

© 2011 Optical Society of America

OCIS codes: (240.6680) Surface plasmons; (250.5403) Plasmonics; (160.5470) Polymers; (130.3120) Integrated optics devices.

References and links

1. H. Raether, *Surface Plasmons* (Berlin, Germany: Springer-Verlag, 1988).
2. N. Fang, H. Lee, C. Sun, and X. Zhang, "Sub-diffraction-limited optical imaging with a silver superlens," Science **308**, 534–537 (2005).
3. M. E. Stewart, C. R. Anderton, L. B. Thompson, J. Maria, S. K. Gray, J. A. Rogers, and R. G. Nuzzo, "Nanostructured Plasmonic Sensors," Chem. Rev. **108**, 494–521 (2008).
4. W.-J. Lee, J.-E. Kim, H. Y. Park, S. Park, J.-M. Lee, M.-s. Kim, J. J. Ju, and M.-H. Lee, "Enhanced Transmission in a Fiber-Coupled Au Stripe Waveguide System," IEEE Photon. Technol. Lett. **22**(2), 100-102 (2010).
5. J. J. Ju, S. Park, M.-s. Kim, J.T. Kim, S. K. Park, Y. J. Park, and M.-H. Lee, "Polymer-Based Long-Range Surface Plasmon Polariton Waveguides for 10-Gbps Optical Signal Transmission Applications," J. Lightwave Technol. **26**, 1510–1518 (2008).
6. R. Charbonneau, N. Lahoud, G. Mattiussi, and P. Berini, "Demonstration of integrated optics elements based on long-ranging surface plasmon polaritons," Opt. Express **13**, 977–984 (2005).
7. A. Boltasseva, T. Nikolajsen, K. Leosson, K. Kjaer, M. S. Larsen, and S. I. Bozhevolnyi, "Integrated optical components utilizing long-range surface plasmon polaritons," J. Lightwave Technol. **23**, 413–422 (2005).
8. H.-R. Park, M.-S. Kim, I.-S. Jeong, J.-M. Park, J. J. Ju, and M.-H. Lee, "Nanoimprinted Bragg Gratings for Long-Range Surface Plasmon Polaritons Fabricated via Spin Coating of a Transparent Silver Ink," IEEE Trans. Nanotechnol. **10**(4), 844-848 (2011).
9. R. Zia, M. D. Selker, P. B. Catrysse, and M. L. Brongersma, "Geometries and materials for subwavelength surface plasmon modes," J. Opt. Soc. Am. A **21**(12), 2442–2446 (2004).

#153295 - $15.00 USD Received 22 Aug 2011; revised 22 Sep 2011; accepted 26 Sep 2011; published 18 Oct 2011

10. J. A. Dionne, L. A. Sweatlock, and H. A. Atwater, "Plasmon slot waveguides: Towards chip-scale propagation with subwavelength-scale localization," Phys. Rev. B, **73**, 035407 (2006).
11. L. Liu, Z. Han, and S. He, "Novel surface plasmon waveguide for high integration, " Opt. Express **13**, 6645–6650 (2005).
12. P. Ginzburg and M. Orenstein, "Plasmonic transmission lines: from micro to nano scale with $\lambda/4$ impedance matching," Opt. Express **15**, 6762–6767 (2007).
13. J. Yoon, S. H. Song, and S. Park, "Flat-top surface plasmon-polariton modes guided by double-electrode structures," Opt. Express **15**, 17151–17162 (2007).
14. D. Woolf, M. Loncar, and F. Capasso, "The forces from coupled surface plasmon polaritons in planar waveguides," Opt. Express **17**, 19996-20011 (2009).
15. P. Ginzburg, D. Arbel, and M. Orenstein, "Gap plasmon polariton structure for very efficient micro-scale-to-nanoscale interfacing," Opt. Lett. **31**, 3288-3290 (2006).
16. S. Zhu, T. Y. Liow, G. Q. Lo, and D. L. Kwong, "Fully complementary metal-oxide-semiconductor compatible nanoplasmonic slot waveguides for silicon electronic photonic integrated circuits," Appl. Phys. Lett. **98**, 021107 (2011).
17. ChemOptics Inc., Available: http://www.chemoptics.co.kr/
18. E. D. Palik, *Handbook of Optical Constants of Solids* (Berlin, Academic, New York, 1985).
19. MODE Solutions, Lumerical Solutions Inc., Available: http://www.lumerical.com/

1. Introduction

Surface plasmon polaritons (SPPs) are transverse magnetic (TM) polarized waves propagating on an interface between a metal and a dielectric [1]. The SPPs arise from the interaction between the evanescent electromagnetic fields and longitudinal collective oscillations of the free electrons in the metal. In general, SPPs support various types of mode properties in diverse structures. Therefore, SPPs have been widely studied for use in micro- to nano-photonic applications [2–13].

On insulator-metal-insulator waveguides (IMI-Ws), a symmetric mode of magnetic fields with respect to the center of the metal, i.e. long-range SPPs (LR-SPPs), can be formed. By controlling the width and the thickness of the metal stripe, the mode-intensity size of the LR-SPP can be easily adjusted to be close to that of a single-mode fiber (SMF) [4–7]. Therefore, the LR-SPP can be efficiently excited by using the butt-coupling method. The propagation length of the LR-SPP dramatically increases with decreasing the metal thickness [4–7]. For these reasons, experimental studies of LR-SPP components including transmission applications, modulators, switches, Y-splitters, directional couplers, and reflection gratings have been widely demonstrated [5–8]. On the other hand, metal-insulator-metal waveguides (MIM-Ws) support a symmetrically coupled mode of magnetic fields with respect to the central insulator layer, which is known as gap-SPP (G-SPP) mode. This G-SPP mode offers high confinement of electromagnetic field in the insulator layer compared to the LR-SPP mode in the IMI-W. The G-SPP mode can be propagated up to the micron-scale length with a nano-scale mode-intensity size by properly adjusting the thickness of the central insulator layer [9–12]. Therefore, mode confinement below the diffraction limit in the MIM-W can be realized in highly integrated photonic devices.

Recently, a more complex multilayered configuration referred to as the insulator-metal-insulator-metal-insulator waveguide (IMIMI-W) has been researched to take advantages of both the IMI-W and MIM-W [9–14]. In the IMIMI-W, the symmetric LR-SPP mode, which is symmetrically coupled with the LR-SPP modes in each metal layer, offers a relatively small mode-intensity size compared to the LR-SPP mode in the IMI-W. On the other hand, the symmetric short range-SPP (SR-SPP) mode, which is symmetrically coupled with the antisymmetric modes in each metal layer, supports a sub-wavelength-size mode similar to the G-SPP mode in the MIM-W. The IMIMI-W can offer hybrid integration and effective mode conversion between the IMI-W and the MIM-W, which results in the benefits of a high integration for more complex plasmonic device geometries with easy fabrication. Furthermore, these hybrid

#153295 - $15.00 USD Received 22 Aug 2011; revised 22 Sep 2011; accepted 26 Sep 2011; published 18 Oct 2011
(C) 2011 OSA

plasmonic waveguides with mode-size converters may be potentially useful for bridging from micro- to nano-photonics.

In general, the coupling loss of light between photonic and plasmonic waveguides which naturally occurs due to the mismatch of modes can be easily minimized by inserting a tapered waveguide [4, 15, 16]. The efficient coupling between different plasmonic waveguides is also essential for hybrid plasmonic integration and can be achieved by introducing a new type of mode-size converter which is presented in this paper. We demonstrate plasmonic mode-size converters (PMSCs) for the effective hybrid integration of IMIMI-W and IMI-W at a telecommunication wavelength. The demonstrated structure was successively composed of the input IMI-W (for reducing the coupling loss with the SMF), a linearly tapered IMIMI-W (LT-IMIMI-W) (for effective squeezing of the LR-SPP mode and reducing the coupling loss between the IMI-W and IMIMI-W [4]), and an IMIMI-W (for propagation of the squeezed LR-SPP mode) in series, which was easily fabricated by using polymer materials and thermal evaporation of gold (Au) with a lift-off technique. The propagation losses, coupling losses and mode-size of each component in the fabricated PMSC were experimentally measured and analyzed.

This paper is organized as follows. In Section 2, the design and fabrication processes of the PMSC are described in detail. The results and discussions are presented in Section 3, while concluding remarks are summarized in Section 4.

2. Design and fabrication processes

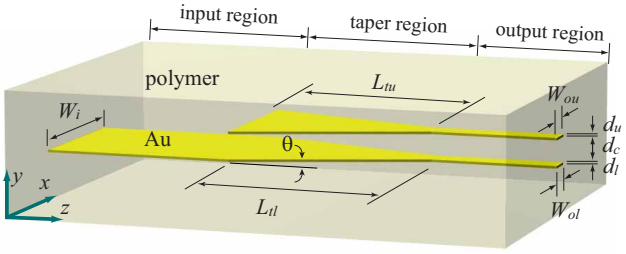

Fig. 1. Schematic view of the proposed PMSC successively composed of an input IMI-W (input region), an LT-IMIMI-W (taper region), and an output IMIMI-W (output region). The width, W_i, of the input region is 6 μm and the width of the output IMIMI-W (W_{ol} and W_{ou}) is 2 or 3 μm. The width of the laterally tapered IMIMI-W of the taper region was linearly varied from W_i to W_{ol}. L_{tl} and L_{tu} denote the lower and upper lengths of the taper region, respectively. The θ denotes the taper angle which depends on the length L_{tl}. Here, the upper stripes in the taper and output regions have the same design parameters of lower stripes. The thicknesses of the Au layers are 14 nm and the central insulator thickness, d_c, is set to 500 nm. The refractive indices for cladding and Au are 1.450 and 0.550 – 11.4912i at the wavelength of 1.55 μm, respectively.

Figure 1 shows the structure of the proposed PMSC consisting of an input IMI-W, an LT-IMIMI-W and an output IMIMI-W. In the input region, in order to reduce the coupling loss between an SMF and the input IMI-W, the width and thickness of the lower Au layer (W_i and d_l) were selected to be 6 μm and 14 nm, respectively [9]. In the taper region, in order to study the lateral taper effect, the lateral tapers with L_{tl} and L_{tu} lengths ranging 1.5 to 240 μm were inserted between the IMI-W and the IMIMI-W [4]. Here, the angles(θ) of the LT-IMIMI-W were calculated based on the taper lengths. In the output region, the width of output IMIMI-W (W_{ol} and W_{ou}) was selected to be 2 or 3 μm. In the taper and output regions, the thickness of the upper Au layer (d_u) was selected to be 14 nm, which is identical to thickness of the lower

#153295 - $15.00 USD Received 22 Aug 2011; revised 22 Sep 2011; accepted 26 Sep 2011; published 18 Oct 2011
(C) 2011 OSA

Au layer to maintain a vertical structural symmetricity [9, 12–14]. The thickness of the central insulator (d_c) was selected to be 500 nm. Here, the refractive indices for the polymeric cladding and Au layers were selected to be 1.450 and 0.550 -11.4912i at the wavelength of 1.55 μm [17, 18].

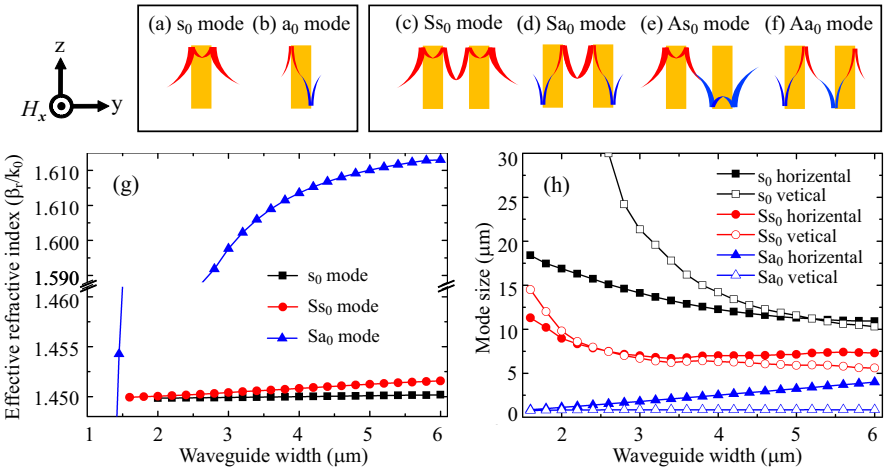

Fig. 2. (a)-(b) s_0 and a_0 modes in the IMI structure. (c)-(f) Ss_0, Sa_0, As_0, and Aa_0 modes in the IMIMI structure. (g) Effective refractive index of the SPP modes as a function of the waveguide width at the wavelength of 1.55 μm. (h) Horizontal and vertical mode-intensity sizes for the s_0 and Ss_0 modes as a function of the waveguide width. The thickness of the Au waveguide is 14 nm and the refractive index of the cladding is 1.45.

The IMI-W supports the two modes of the symmetric mode (s_0, where the subscript 0 indicates the fundamental mode), LR-SPP, and an antisymmetric mode (a_0), SR-SPP, as shown in Figs. 2(a) and 2(b). Here, the symmetric mode is defined as the symmetric field distribution of the transverse magnetic field component (H_x) in the structure. The IMIMI-W supports the two symmetric modes (Ss_0, Sa_0) and the two antisymmetric modes (As_0, Aa_0) as shown in Figs. 2(c)-2(f) [17]. The capital S and A denote the overall symmetric and antisymmetric modes with respect to the central insulator layer, respectively (Figs. 2(c) -2(f)). The Ss_0 mode has optical properties similar to the s_0 mode including propagation loss, mode-intensity size, and mode shape. The optical properties of the Sa_0 mode are similar to the G-SPP mode in the MIM waveguide [9, 10, 12]. In this study, we focused on a mode conversion among the fundamental symmetric modes.

Figure 2(g) shows the effective refractive index of the three SPP modes (s_0, Ss_0, Sa_0) as a function of the lateral IMI-W and IMIMI-W widths, which were calculated using a finite element method. In the 6 μm-wide IMI-W and IMIMI-W, the s_0, Ss_0, and Sa_0 modes can be excited. As shown in Fig. 2(g), the effective refractive indices of the s_0 and Ss_0 modes are very similar. Since the Ss_0 mode is based on the symmetrical two s_0 modes, the field distribution and the mode-size of the Ss_0 mode are closest to those of the s_0 mode, as shown in Figs. 2(a) and 2(c). The power coupling between them is $\sim$0.7 dB, as calculated using the MODE solution from Lumerical Inc. [19]. Therefore, the s_0 mode in the 6 μm-wide IMI-W is most effectively converted into the Ss_0 mode in the 6 μm-wide IMIMI-W. On the other hand, the effective refractive index of the Sa_0 mode is very much different compared to that of the s_0 mode. In addition, the mode-intensity size difference between the s_0 and Sa_0 modes is very large. The power coupling between them calculated using the MODE solution from Lumerical Inc. [19]

#153295 - $15.00 USD Received 22 Aug 2011; revised 22 Sep 2011; accepted 26 Sep 2011; published 18 Oct 2011
(C) 2011 OSA

was ∼40 dB. Therefore, the Sa_0 mode is hard to excite by the s_0 mode passing through the LT-IMIMI-W [4].

As long as the s_0 mode is converted to the Ss_0 mode passing through the LT-IMIMI-W, we expect that the Ss_0 mode in the 3 μm-wide IMIMI-W can be squeezed effectively to ∼40% of the mode-intensity size of the s_0 mode in the 6 μm-wide IMI-W as shown in Fig. 2(h). Here, the horizontal and vertical mode-intensity sizes represent full-width H_x field intensity sizes at the $1/e$ point for each mode. Note that the s_0 mode with the calculated mode-intensity size of 11.0 μm × 10.5 μm (horizontal × vertical) can be converted into the Ss_0 mode with the calculated mode-intensity size of 6.9 μm × 6.6 μm in the 3 μm-wide IMIMI-W, as shown in Fig. 2(h).

The PMSC was fabricated by applying the following procedures. The 30 μm-thick lower cladding was formed onto a Si wafer by spin-coating a polymeric material (ZPU450, Chemoptics Inc., Korea, [17]) with a refractive index of 1.45 at the wavelength of 1.55 μm followed by curing under ultra-violet light (UV, 365 nm) for 5 minutes at the optical power density of 20 mW/cm^2 in a nitrogen atmosphere. Next, the thermally evaporated lower Au stripes with the thickness of 14 nm were fabricated by using lift-off lithography. To form a central insulator layer, a polymeric material (ZPU450(LV500), Chemoptics Inc., Korea, [17])) with an identical refractive index as the lower cladding was spin-coated and UV cured. The thickness of the central insulator layer was measured to be ∼500 nm by a surface profiler. Then, the 14 nm-thick upper Au stripes were fabricated by using the same process applied for the lower Au stripes. The thicknesses of both the lower and upper Au stripes were measured to be ∼14 nm by an atomic force microscope. After forming a 30 μm-thick upper cladding, the fabrication of PMSCs was complete.

3. Results and discussions

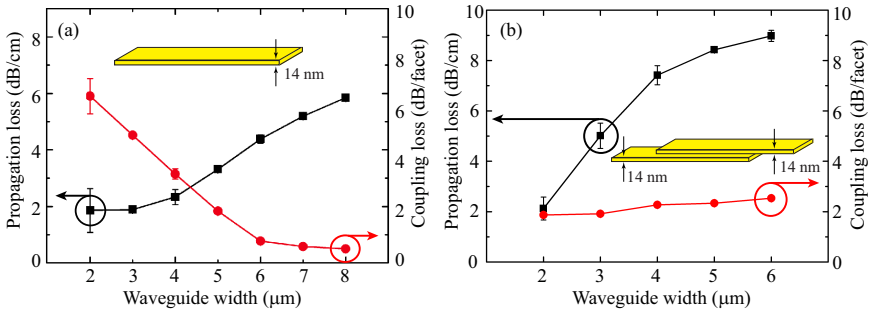

Fig. 3. (a) Propagation loss of the IMI-W and coupling loss between the IMI-W and the PMF at the wavelength of 1.55 μm, as a function of the waveguide width. (b) Propagation losses of the IMIMI-W and coupling loss between the IMIMI-W and the IMI-W. The data points were averaged from two sets of waveguides.

By using the cut-back method, the propagation losses of the 14 nm-thick IMI-Ws and their coupling losses with the polarization-maintaining fiber (PMF) were analyzed from the insertion losses at the wavelength of 1.55 μm. Here, the insertion loss represents the total measured loss of the structure under study, i.e., the total loss between input and output PMFs. The analysis results are shown in Fig. 3(a) as a function of the waveguide width. The propagation loss for the 6 μm-wide IMI-W and its coupling loss with the PMF were 4.38 dB/cm and 0.77 dB/facet, respectively. By using the data of Fig. 3(a) and the partially overlapped IMIMI-Ws in the inset of Fig. 3(b), we also analyzed the propagation losses of the IMIMI-Ws and their coupling losses

#153295 - $15.00 USD Received 22 Aug 2011; revised 22 Sep 2011; accepted 26 Sep 2011; published 18 Oct 2011
(C) 2011 OSA

with the IMI-Ws. The propagation loss for the 3 μm-wide IMIMI-W and its coupling loss with the 3 μm-wide IMI-W were 5.01 dB/cm and 1.92 dB/facet, respectively. Because the IMIMI-W has one more metal layer than the IMI-W, the propagations losses of IMIMI-Ws are larger than those of IMI-Ws at the same waveguide width, as shown in Fig. 3(b). The trends of the propagation loss curves are similar to each other. Because of the increased light reflection at the interface between the IMI-W and the IMIMI-W, the coupling losses between them increased slightly with increasing the waveguide width as shown in Fig. 3(b). Using the results shown in Figs. 2(g), 3(a), and 3(b), the IMI-W (for input and output coupling elements to the PMF) and LT-IMIMI-W (for the coupling element from IMI-W to IMIMI-W) are needed for reducing the coupling loss from PMF to IMIMI-W in order to squeeze the mode-intensity size in the IMIMI-W with a low loss.

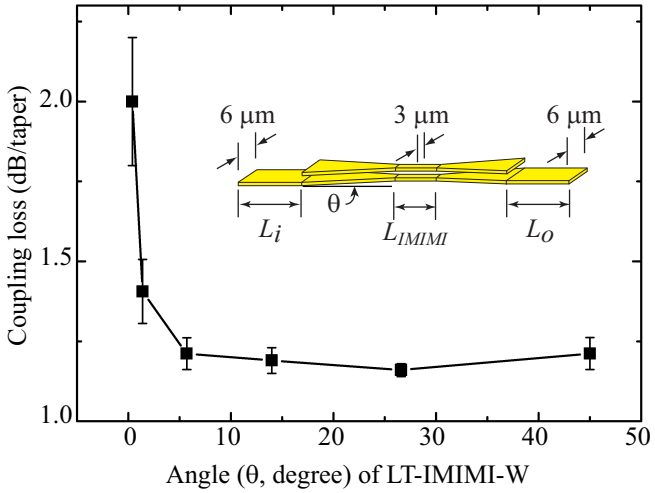

Fig. 4. LT-IMIMI-W coupling losses between 6 μm-wide IMI-W and 3 μm-wide IMIMI-W at the wavelength of 1.55 μm, as a function of the tapered angle (θ). The inset in Fig. 4 represents the bow-tied PMSC for the measurements of the LT-IMIMI-W coupling loss. The data points were averaged from three sets of waveguides.

In order to investigate and analyze the coupling losses of the LT-IMIMI-W introduced between the 6 μm-wide IMI-W and the 3 μm-wide IMIMI-W, a series of bow-tied PMSCs was designed and fabricated as shown in inset of Fig. 4. The insertion losses of the bow-tied PMSCs with a length of 10.5 mm length were measured. Here, the bow-tied PMSCs contained 3 μm-wide IMIMI-W with lengths (L_{IMIMI}) of 2, 3 and 4 mm between the LT-IMIMI-Ws with various tapered angles. The coupling losses ($CL_{LT-IMIMI}$ (dB/taper)) of the LT-IMIMI-W were experimentally determined by using the following Eq. (1):

$$CL_{LT-IMIMI} = (IL_{PMSC} - PL_{IMI} \times (L_i + L_o) - 2 \times CL_{PMF} - PL_{IMIMI} \times L_{IMIMI}) / 2 \quad (1)$$

where IL_{PMSC} is the insertion loss of the bow-tied PMSCs, PL_{IMI} is the propagation loss of the 6 μm-wide IMI-W (see Fig. 3(a)), L_i (L_o) is the total length of the input (output) 6 μm-wide IMI-W (see Fig. 4), CL_{PMF} is the coupling loss between the 6 μm-wide IMI-W and the PMF (see Fig. 3(a)), PL_{IMIMI} is the propagation loss of the 3 μm-wide IMIMI-W (see Fig. 3(b)), L_{IMIMI} is the length of the 3 μm-wid IMIMI-W (see Fig. 4). Here, the denominator 2 comes from the fact that there are two LT-IMIMI-Ws (i.e., two tapers) in the bow-tied PMSCs.

#153295 - $15.00 USD Received 22 Aug 2011; revised 22 Sep 2011; accepted 26 Sep 2011; published 18 Oct 2011
(C) 2011 OSA

The experimentally obtained LT-IMIMI-W coupling losses between the 6 μm-wide IMI-W and the 3 μm-wide IMIMI-W as a function of tapered angle are shown in Fig. 4. Here, the coupling losses include the coupling loss between the 6 μm-wide IMI-W and the 3 μm-wide IMIMI-W as well as the propagation losses for the LT-IMIMI-Ws. With decreasing the angle of the LT-IMIMI-W, which simultaneously results in increasing the length of the LT-IMIMI-W, the coupling losses of the LT-IMIMI-W increase, as shown in Fig. 4. The coupling losses of the LT-IMIMI-W with lengths of less than 1.5 μm (larger than 45°) increased slightly because of stronger light reflection at the interface between the IMI-W and the IMIMI-W [12]. Including the propagation loss of LT-IMIMI-W, the coupling loss of the ∼27° angled LT-IMIMI-W between the 6 μm-wide IMI-W and the 3 μm-wide IMIMI-W is ∼1.16 dB/taper, which was lowest loss obtained, as shown in Fig. 4. In fact, this coupling loss is less than the coupling losses shown in Fig. 3(b) by ∼0.8 dB.

The insertion loss of the bow-tied PMSC composed of two ∼27° angled LT-IMIMI-Ws and the 3 μm-wide IMIMI-W with a 2 mm length is ∼8.6 dB. However, the insertion loss of the partially overlapped IMIMI-W with the 2 mm-long and 3 μm-wide IMIMI-W was ∼15.4 dB, as shown in Fig. 3(b). By using the 6 μm-wide IMI-W (for a coupling element between the PMF and LT-IMIMI-W) and the ∼27° angled LT-IMIMI-W (for a coupling element between the 6 μm-wide IMI-W and 3 μm-wide IMIMI-W), the insertion loss was reduced by ∼6.8 dB. In other words, the coupling loss from the PMF to the 3 μm-wide IMIMI-W was reduced by ∼3.4 dB by using the presented PMSC with a ∼27 ° angled LT-IMIMI-W. These results show that the LT-IMIMI-W is needed to reduce the coupling loss in the PMSC.

Table 1. Comparison of dimensions and losses for the bow-tied PMSC and the partially overlapped IMIMI-W.

	Bow-tied PMSC	Partially overlapped IMIMI-W
Width of IMI-W (μm)	6.0	3.0
Width of IMIMI-W (μm)	3.0	3.0
$L_i + L_o$ (mm)	8.5	8.5
L_{IMIMI} (mm)	2.0	2.0
CL_{PMF} (dB/facet)	0.77	4.52
$CL_{LT-IMIMI}$ (dB/taper)	1.17	-
$CL_{IMI-IMIMI}$ (dB/facet)[a]	-	1.92
Insertion loss (dB)	8.6	15.4
Total coupling loss (dB) [b]	4.3	7.7

[a] $CL_{IMI-IMIMI}$ represents the coupling loss between the IMI-W and the IMIMI-W shown in Fig. 3(b).
[b] Total coupling loss represents a half the insertion loss, i.e., the loss from the input PMF to the IMIMI-W.

Listed in Table 1 is the comparison of dimensions and losses for the bow-tied PMSC and the partially overlapped IMIMI-W. With the shorter length of L_i, we expect that the total coupling loss from the PMF to the 3 μm-wide IMIMI-W for the PMSC can be reduced to ∼2.0 dB.

In order to measure the mode-intensity sizes at the wavelength of 1.55 μm, an IR-Vidicon camera with a 50× objective lens was used to take the images of the mode-intensity. By using a beam view analyzer, the $1/e^2$ horizontal and vertical mode-intensity sizes were evaluated by fitting Gaussian distributions of the captured mode images. The mode-intensity size for the PMF was 10.5 μm × 10.5 μm, as shown in Fig. 5(a). By using butt-coupling method, the s_0 mode in the 6 μm-wide and 14 nm-thick IMI-W was excited and its mode-intensity size was measured to be 13.8 μm × 13.8 μm, as shown in Fig. 5(b). The s_0 mode was coupled into the

#153295 - $15.00 USD Received 22 Aug 2011; revised 22 Sep 2011; accepted 26 Sep 2011; published 18 Oct 2011
(C) 2011 OSA

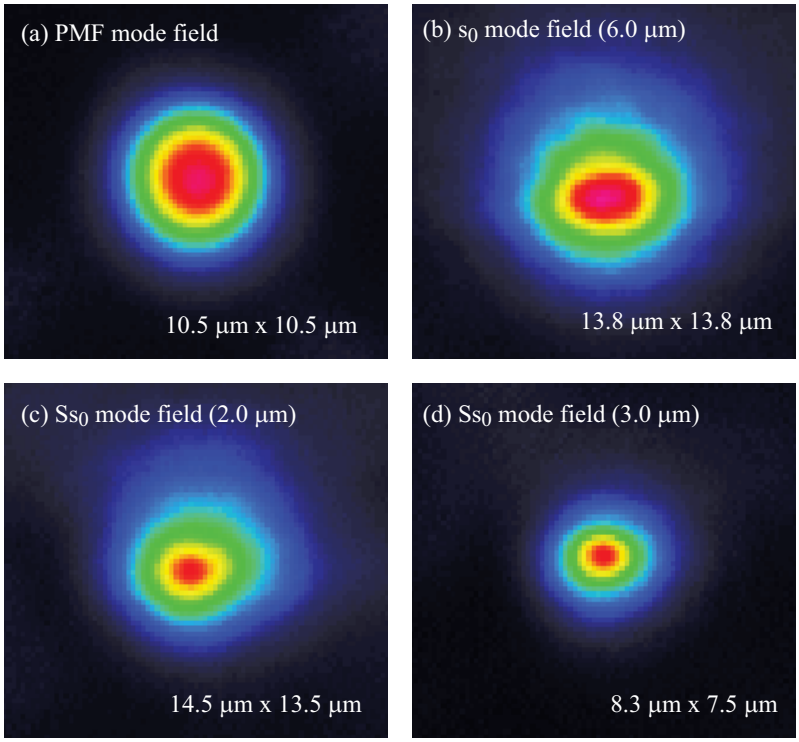

Fig. 5. Optical microscope images of the mode-intensity profiles for the (a) polarization-maintaining fiber (PMF), (b) 6 μm-wide IMI-W, (e) 2 μm-wide IMIMI-W and (f) 3 μm-wide IMIMI-W. An IR-Vidicon camera was used to take the images using a 50$\times$ objective lens. The contour colors represent arbitrary values. The horizontal and vertical mode-intensity sizes were evaluated by fitting Gaussian distributions of the captured mode images.

Ss_0 mode in the 2 and 3 μm-wide IMIMI-Ws via the LT-IMIMI-W, as shown in Fig. 5(c) and 5(d), respectively. The measured mode-intensity sizes for the Ss_0 mode in the 2 and 3 μm-wide IMIMI-W were 14.5 μm $\times$ 13.5 μm and 8.3 μm $\times$ 7.5 μm, respectively. The measured mode-intensity size of the 2 μm-wide IMIMI-W is larger than that of the 3 μm-wide IMIMI-W as expected in Fig. 2(h). Note that the mode-intensity of the Ss_0 mode in the 3 μm-wide IMIMI-W is squeezed to $\sim$35% (horizontal 54% $\times$ vertical 60%) of the s_0 mode in the 6 μm-wide IMI-W.

The use of PMSCs yields advantages of reducing both the insertion loss and the mode-intensity size with easy fabrication. The demonstrated PMSCs can be used as a coupling element from the PMF to micro-plasmonic integrated devices. Moreover, PMSCs may be useful to enhance the efficiency of plasmonic mode converters converting from the micro- to nano-scale SPP mode.

4. Conclusions

In summary, we demonstrated the detailed mode properties of LR-SPPs at the wavelength of 1.55 μm in the presented PMSCs. We both numerically calculated and experimentally measured the mode-intensity sizes of the LR-SPPs for the IMI-W and the IMIMI-W. Moreover, we analyzed the propagation losses of the s_0 mode in the IMI-W and the Ss_0 mode in the

#153295 - $15.00 USD Received 22 Aug 2011; revised 22 Sep 2011; accepted 26 Sep 2011; published 18 Oct 2011
(C) 2011 OSA

IMIMI-W as well as the coupling losses between them. The coupling loss of the $\sim 27^{\circ}$ angled LT-IMIMI-W between the 6 μm-wide IMI-W and the 3 μm-wide IMIMI-W was $\sim$1.16 dB/taper. By using the LT-IMIMI-W, the coupling loss was reduced by $\sim$3.4 dB, which showed that the LT-IMIMI-W is necessary to minimize the insertion loss for the PMSC. In addition, the Ss_0 mode-intensity in the 3 μm-wide IMIMI-W can be reduced to less than 35% of the s_0 mode-intensity in the 6 μm-wide IMI-W. By using the presented PMSC, the s_0 mode in the IMI-W is effectively converted into the Ss_0 mode in the IMIMI-W with a reduction both the insertion loss and the mode-intensity size. In view of the results obtained, the PMSC presented enables effective hybrid integration between the IMI-W and the IMIMI-W. Furthermore, it may be potentially useful for bridging micro- to nano-plasmonic integrated circuits.

Acknowledgments

This work was supported by the IT R&D program of the Ministry of Knowledge Economy (MKE) and the Korea Evaluation Institute of Industrial Technology (KEIT) (KI001804), and the World Class University (WCU) program through the National Research Foundation of Korea (NRF) funded by the Ministry of Education, Science and Technology (MEST) (R32–2008–000–10204–0).

#153295 - $15.00 USD Received 22 Aug 2011; revised 22 Sep 2011; accepted 26 Sep 2011; published 18 Oct 2011
(C) 2011 OSA